---

**Article:**
Fackler, C.J., Xiang, N. and Horoshenkov, K.V. (2018) Bayesian acoustic analysis of multilayer porous media. Journal of the Acoustical Society of America, 144 (6). pp. 3582-3592. ISSN: 0001-4966

https://doi.org/10.1121/1.5083835

---

**Article:**
Fackler, C.J., Xiang, N. and Horoshenkov, K.V. orcid.org/0000-0002-6188-0369 (2018) Bayesian acoustic analysis of multilayer porous media. Journal of the Acoustical Society of America, 144 (6). pp. 3582-3592. ISSN 0001-4966

https://doi.org/10.1121/1.5083835

The Journal of the Acoustical Society of America

# Bayesian acoustic analysis of multilayer porous media

--Manuscript Draft--

| | |
|---|---|
| **Manuscript Number:** | JASA-03359R2 |
| **Full Title:** | Bayesian acoustic analysis of multilayer porous media |
| **Short Title:** | Bayesian analysis for multilayer porous media |
| **Article Type:** | Regular Article |
| **Corresponding Author:** | Ning Xiang, Ph.D.<br>Rensselaer Polytechnic institute<br>Troy, NY UNITED STATES |
| **First Author:** | Cameron J. Fackler, Dr. |
| **Order of Authors:** | Cameron J. Fackler, Dr. |
| | Ning Xiang, Ph.D. |
| | Kirill Horoshenkov, Dr. |
| **Section/Category:** | Noise |
| **Keywords:** | Porous materials, Bayesian inference, Bayesian analysis, inversion, multi-layer materials |
| **Abstract:** | In many acoustical applications, porous materials may be stratified or physically anisotropic along their depth direction. In order to better understand the sound absorbing mechanisms of these porous media, the depth-dependent anisotropy can be approximated as a multilayer combination of finite-thickness porous materials, with each layer being considered as isotropic. The novelty of this work is that it applies Bayesian probabilistic inference to determine the number of constituent layers in a multilayer porous specimen and macroscopic properties of their pores. This is achieved through measurement of the acoustic surface impedance and subsequent transfer-matrix analysis based on an valid theoretical model for the acoustical properties of porous media. The number of layers considered in the transfer-matrix analysis is varied and Bayesian model selection is applied to identify individual layers present in the porous specimen and to infer the parameters of their microstructure. Nested sampling is employed in this process to solve the computationally intensive inversion problem. |

# Bayesian acoustic analysis of multilayer porous media

Cameron J. Fackler,[1] Ning Xiang,[1, a)] and Kirill V. Horoshenkov[2]

[1] *Graduate Program in Architectural Acoustics, Rensselaer Polytechnic Institute, Troy, New York 12180, USA*

[2] *Department of Mechanical Engineering, University of Sheffield, Sheffield, S1 3JD, United Kingdom*

(Dated: 23 November 2018)

In many acoustical applications, porous materials may be stratified or physically anisotropic along their depth direction. In order to better understand the sound absorbing mechanisms of these porous media, the depth-dependent anisotropy can be approximated as a multilayer combination of finite-thickness porous materials, with each layer being considered as isotropic. The novelty of this work is that it applies Bayesian probabilistic inference to determine the number of constituent layers in a multilayer porous specimen and macroscopic properties of their pores. This is achieved through measurement of the acoustic surface impedance and subsequent transfer-matrix analysis based on an valid theoretical model for the acoustical properties of porous media. The number of layers considered in the transfer-matrix analysis is varied and Bayesian model selection is applied to identify individual layers present in the porous specimen and to infer the parameters of their microstructure. Nested sampling is employed in this process to solve the computationally intensive inversion problem.

[a)]xiangn@rpi.edu

## I. INTRODUCTION

Modelling of the acoustical properties of porous materials is used extensively in a range of engineering and science applications. In outdoor sound propagation and seismic studies, soil and sediment may be represented as multilayered porous media (Sabatier *et al.*, 1986; Sabatier and Xiang, 2001). Similarly, marine sediments may be considered as porous media, with pores saturated with water rather than air (Buckingham, 2000; Leurer and Brown, 2008). In architectural acoustics and noise control engineering, porous materials are traditionally used to absorb an excess or unwanted acoustic energy. In performance venues, the reverberant sound field may be controlled with porous absorbers to optimize the space for various types of musical performances (Beranek, 2004). In industrial spaces and office buildings, porous materials control the level of noise to enhance speech intelligibility and provide privacy, to ensure a reasonable office environment (Jeong *et al.*, 2017; Long, 2014).

In all cases, the microscopic properties of a material's pores govern the material's acoustic behavior (Chevillotte *et al.*, 2015), and it is of importance to understand this relation. Estimating these macroscopic properties from the acoustical data is of interest in the physical study of soils (Sabatier *et al.*, 1986) and ground coverings (Attenborough, 1985; Horoshenkov *et al.*, 2013) and underwater sediments (Buckingham, 2000; Leurer and Brown, 2008). From the architectural acoustics and noise control standpoint, these parameters can be used to predict and design new types of porous media with a higher acoustic absorption performance than existing commercial absorbers (Mahasaranon *et al.*, 2012). An understanding of these parameters' interdependence may lead to the development of new sound absorbing materials

or new applications of acoustics to measure non-invasively the microstructure of new types of porous media.

This paper applies Bayesian probabilistic inference to the analysis of multilayered porous media to invert the macroscopic material properties from acoustic impedance data, whereas direct measurement (see, for example, Allard and Atalla, 2009) of these parameters is often time-consuming or impossible. The proposed inversion method efficiently determines all the microscopic parameters from a single acoustical measurement on a small material specimen. Given a theoretical model for the acoustic response of a porous material, an inverse problem may be solved probabilistically to determine the material physics from a measurement of the material's acoustic response. This approach is an efficient alternative to other inversion methods which are based on direct optimization (e.g. Atalla and Panneton, 2005; Ogam *et al.*, 2010) or asymptotic limits (e.g. Allard *et al.*, 1994).

Recent studies have applied Bayesian parameter estimation approaches for the characterization of single-layered porous materials Chazot *et al.* (2012); Niskanen *et al.* (2017). In both cases, a Bayesian method is used to determine inversely the physical parameters of a porous material, from an acoustical measurement of the porous specimen in an impedance tube. The present work represents an enhancement to these methods, because the Bayesian framework investigated in the current work includes a model selection component to determine the number of layers present in a material specimen under test in addition to porous parameter estimation. Thus the method is not limited to the characterization of single-layer specimens. Additionally, the prior probabilities for inverted parameters are assigned

to be broad, uninformative distributions, so that the inverted parameter values are based predominantly on the measured acoustic data.

In addition to the parameter estimation problems discussed above, Bayesian model selection has found recent applications throughout acoustics. Xiang (2015); Xiang and Goggans (2003) apply model selection to determine the number of coupled spaces present in an acoustic space by analyzing sound energy decay functions. In the context of acoustic localization, Bush and Xiang (2018); Escolano *et al.* (2012, 2014) determine the number of simultaneous sound sources present with an application Bayesian model selection. Battle *et al.* (2004); Dettmer *et al.* (2009, 2010) apply Bayesian model selection to geoacoustic inversion, to the study of water-saturated sediment layers on the seabed. Bayesian model selection has also been applied to room-acoustic modal analysis (Beaton and Xiang, 2017) and to the design of digital filters for signal processing (Botts *et al.*, 2013; Chan and Goggans, 2012). However, to the best of the author's knowledge, the tool of Bayesian model selection has not yet been applied to the study of multilayer air-saturated acoustic porous materials.

The remainder of this paper is organized as follows. Section II discusses the theory of modeling and measuring the acoustic properties of multilayer porous materials. The generalized Miki model for porous media is presented, along with a transfer-matrix multilayer modeling framework. Next, Section III develops the Bayesian probabilistic framework used to perform the inverse analysis. Section IV presents the results obtained from analyzing realistic multilayer porous material samples, and Section V concludes the paper.

## II. POROUS MEDIA MODEL

Sound wave propagation in the porous layers can be described by a set of physical parameters. Stacking multiple distinct layers with each layer having different sets of porous parameters can be collectively described by the transfer matrix method. This Section introduces a multi-layered model of porous media, which is used in the model-based Bayesian analysis in Sec. III.

### A. Miki Generalized Model

This work applies the semi-empirical model by Miki (1990) to relate the acoustical and microscopic properties of porous media. This model is attractive because it is robust. It represents an improvement to the well-known Delany and Bazley (1970) model in terms of its causality and behavior in the low-frequency limit. Miki (1990) developed the theoretical expressions for the flow resistivity $\sigma_f$, porosity $\phi$, and tortuosity $\alpha_\infty$ of a porous material comprising cylindrical tubes oriented at an arbitrary angle to the surface normal. From these expressions, the propagation coefficient (also known as propagation constant or complex wavenumber) and characteristic impedance for materials with tortuous pores and porosities less than unity were derived. According to the Miki (1990) generalized empirical model, the propagation coefficient, $\gamma$, and characteristic impedance, $Z_c$, are given as:

$$\gamma(f) = \frac{2\,\pi\,f\sqrt{\alpha_\infty}}{c_0}\left(0.160\left(\frac{f}{\sigma_e}\right)^{-0.618} + i\left[1 + 0.109\left(\frac{f}{\sigma_e}\right)^{-0.618}\right]\right), \tag{1}$$

and

$$Z_c(f) = \rho_0 c_0 \frac{\sqrt{\alpha_\infty}}{\phi}\left(1 + 0.070\left(\frac{f}{\sigma_e}\right)^{-0.632} - i0.107\left(\frac{f}{\sigma_e}\right)^{-0.632}\right), \tag{2}$$

respectively, with

$$\sigma_e = \frac{\phi}{\alpha_\infty}\sigma_f \tag{3}$$

being the effective flow resistivity of the porous material. $\rho_0$ and $c_0$ are respectively the density and sound speed of the pore-saturating fluid, and $i = \sqrt{-1}$.

### B. Multilayer Model: Transfer Matrix Method

When combining multiple distinct layers into a multilayered material, the transfer matrix method may be used to model the overall behavior of the material. The transfer matrix method represents each homogeneous layer of a multilayer material with a transfer matrix, which relates the acoustic field quantities at the front and rear interfaces of each layer. The following is a summary of the transfer matrix method for modeling multilayer equivalent-fluid materials, as in Allard and Atalla (2009).

For the materials discussed in this work, each layer may be modeled as an equivalent fluid whose properties are predicted by the Miki (1990) generalized model. In this case, a two-by-two transfer matrix relates the acoustic pressure and normal component of particle velocity between the two sides of each layer. As modeled in this work, the transfer matrix

for an equivalent fluid layer of thickness $d$ is given as:

$$\mathbf{T}_{\text{eq}} = \begin{bmatrix} \cosh(\gamma d) & \sinh(\gamma d) \cdot Z_c \\ \sinh(\gamma d)/Z_c & \cosh(\gamma d) \end{bmatrix}, \tag{4}$$

where $\gamma$ is the propagation coefficient of the equivalent fluid as given in Equation (1) and $Z_c$ is the characteristic impedance as given in Equation (2). In general, these quantities are complex valued functions of frequency for an equivalent fluid layer.

For a rigid-backed equivalent-fluid layer, oriented normal to the $x$-direction with the sound propagation being along the $x$-direction, the transfer matrix is applied to model the acoustic quantities at the front surface of the layer as:

$$\begin{bmatrix} p \\ v_x \end{bmatrix}_{x=0} = \mathbf{T}_{\text{eq}} \begin{bmatrix} 1 \\ 0 \end{bmatrix}, \tag{5}$$

where $p$ is the acoustic pressure, $v_x$ is the normal component of the acoustic particle velocity, and the subscript $x = 0$ indicates the front material surface.

In case of a material composed of $Q$ equivalent-fluid layers, the single transfer matrix is replaced by a chain of two-by-two transfer matrices, with one matrix in Equation (4) for each distinct layer. Equation (5) is modified, resulting in:

$$\begin{bmatrix} p \\ v_x \end{bmatrix} = \mathbf{T}_{\text{eq}}^{(1)} \times \mathbf{T}_{\text{eq}}^{(2)} \times \cdots \times \mathbf{T}_{\text{eq}}^{(N)} \times \begin{bmatrix} 1 \\ 0 \end{bmatrix}, \tag{6}$$

where the superscript $(n)$ denotes the transfer matrix for the $n$-th equivalent fluid layer computed using Equation (4), and $\times$ is the matrix product. The material layers (and corresponding transfer matrices) are arranged with layer 1 being the front and layer $N$ being

adjacent to the rigid backing. Here, $p$ and $v_x$ are the acoustic pressure and surface-normal acoustic particle velocity at the front surface of the multilayer structure. Consequently, the normal-incidence surface impedance for the multilayer material is modeled as:

$$Z_s = \frac{p}{v_x}. \tag{7}$$

This multi-layered porous material model is used in the Bayesian model-based inversion in the following, involving the normal-incidence acoustic surface impedance of potentially multilayered materials experimentally measured with the standard impedance tube method (Chung and Blaser, 1980; International Standards Organization, 1998).

## III. BAYESIAN INFERENCE FRAMEWORK

In the Bayesian interpretation of probability theory, probabilities represent and quantify states of knowledge or degrees of belief (Xiang and Fackler, 2015). Bayesian inference is a framework for drawing conclusions from measured data, where probabilities quantify the knowledge gained. In Bayesian inference, Bayes' theorem is used to update knowledge about quantities of interest, given relevant data or observations.

### A. Bayes' theorem

At the heart of Bayesian inference is Bayes' theorem, which in its most general form relates the probabilities for two general propositions $A$ and $B$. In the Bayesian interpretation, the probability of a proposition quantifies the state of knowledge about that proposition. Examples could include the likelihood of a given result from all potential event outcomes

or the particular value of a parameter within a set or range of possible values. With $\Pr(\bullet)$ denoting a probability distribution, Bayes' theorem is written as:

$$\Pr(A \,|\, B) = \frac{\Pr(A)\ \Pr(B \,|\, A)}{\Pr(B)}, \tag{8}$$

where $\Pr(A)$ and $\Pr(B)$ describe the probabilities of propositions $A$ and $B$, respectively. Probabilities of the form $\Pr(A \,|\, B)$ are *conditional* probabilities, in this case of proposition $A$ given that proposition $B$ is fixed at a given outcome or value. Bayes' theorem is easily derived from the product rule of conditional probability. Expanding $\Pr(A, B)$, the *joint* probability of $A$ and $B$, which quantifies the full state of knowledge of both propositions, including any ways in which they influence each other, yields:

$$\Pr(A, B) = \Pr(A \,|\, B)\ \Pr(B) = \Pr(B \,|\, A)\ \Pr(A), \tag{9}$$

leading to Equation (8) after a simple rearrangement.

In the context of the Bayesian data analysis and model-based inference reported in this work, Bayes' theorem is often written as:

$$\Pr(H \,|\, \boldsymbol{\mathcal{D}}, I) = \frac{\Pr(H \,|\, I)\ \Pr(\boldsymbol{\mathcal{D}} \,|\, H, I)}{\Pr(\boldsymbol{\mathcal{D}} \,|\, I)}, \tag{10}$$

where $H$ represents a conjecture or hypothesis, $\boldsymbol{\mathcal{D}}$ represents experimental observations or data, and $I$ represents available relevant, testable background information. The hypothesis $H$ may represent either a model or a set of parameters, depending on the problem at hand, as discussed in the following sections. Each $\Pr(\bullet)$ term in Bayes' theorem is a probability, each serving a different function and commonly referred to by a different name representative of its function.

The term $\Pr(H \mid I)$ represents the state of knowledge about the hypothesis $H$ at the beginning of the analysis. This *prior* distribution is conditioned on any knowledge or information available before experimental data are incorporated into the analysis. The probability $\Pr(\boldsymbol{\mathcal{D}} \mid H, I)$ is known as the *likelihood* function and indicates the plausibility that the measured data $\boldsymbol{\mathcal{D}}$ would have been generated, given that the hypothesis $H$ is true. This likelihood function serves to update the prior knowledge once the experimental data have been measured or observed. When applying the Bayesian framework to solve an inference problem, the prior and likelihood serve as inputs to the computation and are assigned before any data are observed (Xiang and Fackler, 2015).

The *posterior* distribution, $\Pr(H \mid \boldsymbol{\mathcal{D}}, I)$, encodes the state of knowledge that results from updating the prior knowledge with measured data via the likelihood function. In order for the posterior to be a proper probability density function, its volume must be normalized to unity. The term $\Pr(\boldsymbol{\mathcal{D}} \mid I)$ is called the *(Bayesian) evidence* and serves as the posterior normalization constant. As demonstrated in Section III B 1, the evidence is also important for applications of Bayesian model selection.

## B. Two Levels of Bayesian Inference

Bayesian probabilistic inference encompasses both parameter estimation and model selection problems. Bayesian inference applied to solving parameter estimation problems is referred to as the first (low) level of inference, while application of Bayes' theorem to solving model selection problems is referred to as the second (high) level of inference (e.g. (Jefferys and Berger, 1992; Xiang, 2015)). Using a top-down approach, the following discussion begins

with the so-called second level of inference, model selection, before proceeding to parameter estimation. The discussion proceeds under the basis that one should determine which of a set of competing models is appropriate before the relevant model parameters are inferred using that model.

### *1. Model Selection: Second Level of Inference*

In the context of model-based inference, an appropriate model is required to predict the data at hand. However, given a set of competing models, the model that best fits the data is not necessarily the best choice for inference. More complex models (in the present work, for example, multilayer models with increasing numbers of material layers) are capable of fitting the data as well as or better than simpler models, but often generalize poorly, leading to overfitting or modeling noise inherent to the data (Jefferys and Berger, 1992; MacKay, 2003).

The Bayesian model selection process applies Bayes' theorem to the task of choosing a model for use in drawing further inferences, with the model to be selected serving as the hypothesis of Equation (10). The model is selected from a finite set of $N$ models, $\boldsymbol{\mathcal{M}} = \{\mathcal{M}_1, \ldots, \mathcal{M}_N\}$, each of which is a function of a corresponding parameter set and is known to be a candidate to describe the data $\boldsymbol{\mathcal{D}}$ well. In the present context of multilayer porous media analysis, each of the $N$ models in $\boldsymbol{\mathcal{M}}$ comprises a different number of material layers, from 1 to $N$. The parameter set for each layer consists of the physical parameters of flow resistivity $\sigma_f$, porosity $\phi$, tortuosity $\alpha_\infty$, and layer thickness $d$. Each model $\mathcal{M}_n$ is the

multilayer transfer matrix formulation of the generalized Miki model (as described above in Section II) with $n$ equivalent-fluid layers and is a function of $4n$ physical parameters.

Bayes' theorem applied to each model $\mathcal{M}_n$ in the finite set of $N$ competing models, $\boldsymbol{\mathcal{M}}$, is written as:

$$\Pr(\mathcal{M}_n \,|\, \boldsymbol{\mathcal{D}}, I) = \frac{\Pr(\mathcal{M}_n \,|\, I)\ \Pr(\boldsymbol{\mathcal{D}} \,|\, \mathcal{M}_n, I)}{\Pr(\boldsymbol{\mathcal{D}} \,|\, I)}, \tag{11}$$

In the form of Equation (11), Bayes' theorem represents how one's prior knowledge about the model $\mathcal{M}_n$, expressed by *prior probability* $\Pr(\mathcal{M}_n \,|\, I)$, is updated in the presence of data $\boldsymbol{\mathcal{D}}$, given the background information $I$. The *likelihood* of the data having been generated, given a particular model $\mathcal{M}_n$, is notated $\Pr(\boldsymbol{\mathcal{D}} \,|\, \mathcal{M}_n, I)$, while $\Pr(\mathcal{M}_n \,|\, \boldsymbol{\mathcal{D}}, I)$ is the *posterior probability* of the model $\mathcal{M}_n$ given the data.

The model comparison between two different models $\mathcal{M}_i$ and $\mathcal{M}_j$ evaluates the so-called Bayes' factor $\mathcal{K}_{i,j}$ (Kass and Raftery, 1995):

$$\begin{aligned} \mathcal{K}_{i,j} &= \frac{\Pr(\mathcal{M}_i \,|\, \boldsymbol{\mathcal{D}}, I)}{\Pr(\mathcal{M}_j \,|\, \boldsymbol{\mathcal{D}}, I)} \\ &= \frac{\Pr(\boldsymbol{\mathcal{D}} \,|\, \mathcal{M}_i, I)}{\Pr(\boldsymbol{\mathcal{D}} \,|\, \mathcal{M}_j, I)}\ \frac{\Pr(\mathcal{M}_i \,|\, I)}{\Pr(\mathcal{M}_j \,|\, I)}, \end{aligned} \tag{12}$$

where $1 \leq i, j \leq N$; $i \neq j$. In the right-hand side of the Bayes' factor, the second fraction, termed the prior ratio, represents how much model $\mathcal{M}_i$ is preferred over $\mathcal{M}_j$ before considering the data $\boldsymbol{\mathcal{D}}$. If one wants to incorporate no prior preference assigning equal prior probability:

$$\Pr(\mathcal{M}_n \,|\, I) = \frac{1}{N}, \quad 1 \leq n \leq N \tag{13}$$

to each of $N$ models, then no subjective preference is encoded for any of these models. In this case, the Bayes' factor for the model comparison between two different models $\mathcal{M}_i$ and

$\mathcal{M}_j$ relies solely on the posterior ratio between models:

$$\mathcal{K}_{i,j} = \frac{\Pr(\boldsymbol{\mathcal{D}} \,|\, \mathcal{M}_i, I)}{\Pr(\boldsymbol{\mathcal{D}} \,|\, \mathcal{M}_j, I)}, \; 1 \leq i, j \leq N; \; i \neq j, \tag{14}$$

which is equal to the likelihood ratio when the model prior probabilities are uniform. This indicates that the likelihood $\Pr(\boldsymbol{\mathcal{D}} \,|\, \mathcal{M}_n, I)$ plays a central role in Bayesian model selection. In the following section, it will be shown that this likelihood term in the context of model selection is identical to the *evidence* term in the context of parameter estimation.

Since the Bayes factor is a ratio of likelihoods, it may be expressed in log odds and quantified using units of information or entropy. In particular, using base-10 logarithms, the Bayes factor may be expressed in decibans (unit dBans, also called decihartleys) as $10 \cdot \log_{10}(\mathcal{K}_{i,j})$. The second level of Bayesian inference intrinsically embodies Occam's razor (Jefferys and Berger, 1992) in a quantitative way. Complicated models are penalized and assigned large probabilities only if the complexity of the data justifies the additional model complexity (Jefferys and Berger, 1992; MacKay, 2003).

### *2. Parameter Estimation: First Level of Inference*

Once a model $\mathcal{M}_n$ has been chosen via the model selection, it may be used to infer the values of the parameters that describe the measured data. For the purpose of parameter estimation, Bayes' theorem is applied with the parameters $\boldsymbol{\theta}_n$ serving as the hypothesis. In this context, the background information $I$ includes that a specific model $\mathcal{M}_n$ is given or selected via the model selection, and the model describes the data $\boldsymbol{\mathcal{D}}$ well. The subscript $n$ emphasizes that the model, $\mathcal{M}_n(\boldsymbol{\theta}_n)$, is a function of the particular parameter set. Bayes'

theorem for this parameter estimation problem is written as:

$$\Pr(\boldsymbol{\theta} \,|\, \boldsymbol{\mathcal{D}}, \mathcal{M}) = \frac{\Pr(\boldsymbol{\theta} \,|\, \mathcal{M})\ \Pr(\boldsymbol{\mathcal{D}} \,|\, \boldsymbol{\theta}, \mathcal{M})}{\Pr(\boldsymbol{\mathcal{D}} \,|\, \mathcal{M})}, \tag{15}$$

where the subscript $n$ and background information $I$ have been dropped for simplicity. Bayes' theorem used in this problem represents how one's prior knowledge about parameters $\boldsymbol{\theta}$, given the specific model $\mathcal{M}(\boldsymbol{\theta})$, is updated in the presence of data $\boldsymbol{\mathcal{D}}$.

The prior $\Pr(\boldsymbol{\theta} \,|\, \mathcal{M})$ encodes all that is known about the parameters before incorporating the data and is notated as $\Pi(\boldsymbol{\theta}) \equiv \Pr(\boldsymbol{\theta} \,|\, \mathcal{M})$ for simplicity. Once the data have been observed or measured, the likelihood $\Pr(\boldsymbol{\mathcal{D}} \,|\, \boldsymbol{\theta}, \mathcal{M})$ incorporates the data to update the prior knowledge of the parameters. To emphasize that the data are fixed once observed and that the likelihood is therefore a function of the parameter values, it is notated as $\mathcal{L}(\boldsymbol{\theta}) \equiv \Pr(\boldsymbol{\mathcal{D}} \,|\, \boldsymbol{\theta}, \mathcal{M})$.

The posterior $\Pr(\boldsymbol{\theta} \,|\, \boldsymbol{\mathcal{D}}, \mathcal{M})$ quantifies the updated knowledge of the parameters; as a proper probability density function, it must integrate to unity over the entire parameter space. With the notational changes of the previous paragraph, this normalization constraint is enforced by integrating both sides of Equation (15) over the entire parameter space, yielding

$$1 = \int_{\boldsymbol{\theta}} \Pr(\boldsymbol{\theta} \,|\, \boldsymbol{\mathcal{D}}, \mathcal{M})\, d\boldsymbol{\theta} = \int_{\boldsymbol{\theta}} \frac{\mathcal{L}(\boldsymbol{\theta})\, \Pi(\boldsymbol{\theta})}{\Pr(\boldsymbol{\mathcal{D}} \,|\, \mathcal{M})}\, d\boldsymbol{\theta}. \tag{16}$$

Lacking any dependence on the parameter values, the denominator of the right hand side may be taken out of the integral, leading to the posterior normalization condition being specified as:

$$\Pr(\boldsymbol{\mathcal{D}} \,|\, \mathcal{M}) \equiv \mathcal{Z} = \int_{\boldsymbol{\theta}} \mathcal{L}(\boldsymbol{\theta})\, \Pi(\boldsymbol{\theta})\, d\boldsymbol{\theta}, \tag{17}$$

where $\mathcal{Z} \equiv \Pr(\boldsymbol{\mathcal{D}} \,|\, \mathcal{M})$ is the Bayesian *evidence* for model $\mathcal{M}$ (MacKay, 2003). Referring to the previous section, the evidence is exactly the same as the likelihood in Equations (11) and (14). In addition to its function as the parameter estimation posterior normalization constant, this evidence also plays a central role in model selection (MacKay, 2003; Xiang, 2015).

Rearranging the term of Equation (15) yields (Skilling, 2006):

$$\begin{aligned} \Pr(\boldsymbol{\theta} \,|\, \boldsymbol{\mathcal{D}}, \mathcal{M}) \times \quad \mathcal{Z} \quad &= \Pi(\boldsymbol{\theta}) \times \quad \mathcal{L}(\boldsymbol{\theta}), \\ \text{posterior} \quad \times \text{evidence} &= \text{prior} \times \text{likelihood}, \end{aligned} \tag{18}$$

which states the logical relationship among the quantities of Bayesian inference. The prior probability $\Pi(\boldsymbol{\theta})$ and the likelihood function $\mathcal{L}(\boldsymbol{\theta})$ are the inputs, while the posterior probability $\Pr(\boldsymbol{\theta} \,|\, \boldsymbol{\mathcal{D}}, \mathcal{M})$ and the evidence $\mathcal{Z}$ are the outputs of Bayesian inference. Particularly, the posterior probability is the output for the first level of inference, parameter estimation, while the evidence $\mathcal{Z}$ is the output for the second level of inference, model selection. Bayesian evidence automatically encapsulates the principle of parsimony and quantitatively embodies Occam's razor (Jefferys and Berger, 1992; MacKay, 2003). When two competing theories explain the data equally, the simpler one is preferred.

### C. Parameter priors

Before any data have been observed, limited knowledge is available about the parameters under study. To begin a Bayesian analysis, this limited knowledge must be encoded into the prior probability distribution for each parameter.

For realistic porous materials, the physical parameters describing the pore structure fall into broad ranges of physically realistic values. Following the principle of maximum entropy and applying the transformation-group arguments of Jaynes (1968), a uniform prior distribution is assigned to each of the physical porous material parameters. Using realistic parameter value ranges, the following priors are assigned, encoding a lack of specific prior knowledge:

$$\Pr(\text{flow resist.}\sigma_f) = \text{Uniform}(0.1, 1000 \text{ kNs/m}^4), \tag{19}$$

$$\Pr(\text{porosity } \phi) = \text{Uniform}(0.1, 1), \tag{20}$$

$$\Pr(\text{tortuosity } \alpha_\infty) = \text{Uniform}(1, 7). \tag{21}$$

For the materials used in this work, the material layers considered are on the order of a few centimeters thick. To remain impartial when considering the layer thickness as an unknown parameter, a broad range is considered for the thickness. Thus, when the thickness is a parameter to be estimated, it is assigned the following prior,

$$\Pr(\text{layer thickness } d) = \text{Uniform}(0.1 \text{ mm}, 10 \text{ cm}); \tag{22}$$

otherwise, it is fixed at the physically-measured value. If the present methods were to be applied to conditions in which the layer thicknesses are truly unknown, an even more conservative (larger) prior range may be warranted.

### D. Likelihood function

The squared error between measured ($Z_{s,\text{meas}}$) and modeled ($Z_{s,\text{mod}}$) complex surface impedance data is given as:

$$E_b^2 = \text{Re}(Z_{s,\text{meas},b} - Z_{s,\text{mod},b})^2 + \text{Im}(Z_{s,\text{meas},b} - Z_{s,\text{mod},b})^2, \tag{23}$$

at each measured frequency point $b$, where the real and imaginary parts of the complex surface impedance are considered separately. For use in the Bayesian inference framework, this error must be assigned a probability. As stated previously for Equation (15) in Section III B 2, the background information includes the model being chosen to predict the measured data sufficiently well, which implies that the mean error across data points should be around 0, while the variance in error values must be finite. Applying the principle of maximum entropy given these constraints, the likelihood function is assigned as a Student's $t$-distribution (Jasa and Xiang, 2009)

$$\mathcal{L}(\boldsymbol{\theta}) = \Pr(\boldsymbol{\mathcal{D}} \,|\, \boldsymbol{\theta}, \mathcal{M}) = \frac{\Gamma(B/2)}{2} \left( \pi \sum_{b=1}^{B} E_b^2 \right)^{-B/2}, \tag{24}$$

where the squared errors $E_b^2$ given in Equation (23) have been summed across all $B$ measured frequency points, and $\Gamma(\bullet)$ is the Gamma function.

### E. Nested sampling

The evidence $\mathcal{Z}$ in Equation (17) and Equation (18) is the most important quantity for the two levels of Bayesian inference (MacKay, 2003). Nested sampling (Skilling, 2004, 2006)

is a numerical algorithm for estimating the evidence in a Bayesian inference problem, using the prior and likelihood as inputs and generating samples from the posterior as a secondary output. Recent applications of the nested sampling in Bayesian analysis in acoustics can also be found in Beaton and Xiang (2017); Bush and Xiang (2018); Escolano *et al.* (2014).

Nested sampling exploits the close relationship between the likelihood function $\mathcal{L}(\boldsymbol{\theta})$ and the constrained prior mass $\varepsilon(\lambda)$, defined as:

$$\varepsilon(\lambda) = \iint\cdots\int_{\mathcal{L}(\boldsymbol{\theta})>\lambda} \Pi(\boldsymbol{\theta})\, d\boldsymbol{\theta}, \tag{25}$$

which is the amount (mass) of the prior density $\Pi(\boldsymbol{\theta})$ contained in the parameter space where the value of the likelihood function $\mathcal{L}(\boldsymbol{\theta})$ is greater than a constraining value $\lambda$. With this definition, the evidence, which is a multidimensional integral over the entire parameter space, is mapped to a single-dimensional integral over the constrained prior mass:

$$\mathcal{Z} = \iint\cdots\int \mathcal{L}(\boldsymbol{\theta})\,\Pi(\boldsymbol{\theta})\, d\boldsymbol{\theta} = \int_0^1 \mathcal{L}(\varepsilon)\, d\varepsilon, \tag{26}$$

where $\mathcal{L}(\varepsilon)$ is the likelihood value bounding the region of the parameter space within which $\varepsilon$ prior mass is constrained. In other words, when considering the constrained prior mass as defined in Equation (25), the constraining likelihood value is $\lambda = \mathcal{L}(\varepsilon)$. Note that $\mathcal{L}(\varepsilon)$ is the likelihood value bounding a region of the parameter space, whereas $\mathcal{L}(\boldsymbol{\theta})$ is the likelihood function evaluated at a given set of parameter values $\boldsymbol{\theta}$.

As a further point of clarification, consider the two limits of integration in the right hand side of Equation (26). At $\varepsilon = 1$ the entire prior mass is constrained, corresponding to the entire parameter space, and thus the constraining likelihood is the minimum likelihood

value: $\mathcal{L}(\varepsilon = 1) = \mathcal{L}_{\min} \geq 0$. At the other limit, $\varepsilon = 0$ corresponds to no constrained prior mass, which occurs at the single point of maximum likelihood value: $\mathcal{L}(\varepsilon = 0) = \mathcal{L}_{\max}$.

The nested sampling procedure starts with a population of $Q$ sample objects, which are sampled according to the prior density (see Equations (19)–(22)). Since the initial samples are distributed across the entire parameter space, initially the entire prior density is considered to be constrained yielding

$$\varepsilon_0 \approx 1 \tag{27}$$

and the initial constraining likelihood value is

$$\mathcal{L}_0 \approx 0. \tag{28}$$

At the $k$-th step of the iterative procedure, the sample (corresponding to parameter values $\boldsymbol{\theta}_k$) in the population of $Q$ corresponding to the lowest likelihood value (stored as $\mathcal{L}_k$) is first recorded then discarded. A constraint is created by this likelihood; specifically, the likelihood values of the surviving $Q - 1$ samples that are greater than that of the discarded sample. The discarded sample is then replaced by a new sample, constrained to have a likelihood value greater than that of the discarded sample. The new sample may be generated by evolving an existing sample that already satisfies the likelihood constraint, such as with a random-walk Metropolis-Hastings procedure (Skilling, 2006), a constrained Hamiltonian Monte Carlo method (Betancourt, 2011), or others. After generation of a replacement sample, a population of $Q$ samples exists which are distributed uniformly over the prior mass constrained by the limiting likelihood value $\mathcal{L}_k$ of the discarded sample. For a population of $Q$ samples, the constrained prior mass will tend to shrink exponentially by

1 part in $Q$ at each iteration, leading to:

$$\varepsilon_k \approx \exp\left(-\frac{k}{Q}\right). \tag{29}$$

After each iteration, the parameter values $\boldsymbol{\theta}_k$ of the discarded sample and the values of $\mathcal{L}_k$ and $\varepsilon_k$ are accumulated. The nested sampling process may be thought of as accumulating the evidence across the parameter space, iteratively estimating the integral of Equation (26) as the population of samples approaches the region of maximum likelihood. At any iteration $k$, the population of live samples contains an amount of "live" evidence that has yet to be accumulated (Keeton, 2011). By averaging the constrained prior over the remaining samples, this live evidence may be estimated by:

$$\mathcal{Z}_k = \frac{1}{Q}\sum_{q=1}^{Q} \mathcal{L}_q\, \varepsilon_k, \tag{30}$$

where $\mathcal{L}_q$ is the likelihood value of the $q$-th live sample and the sum is over the $Q$ samples in the population.

The nested sampling procedure terminates after $K$ iterations. This termination may be based on any of various criteria (e.g. Sivia and Skilling, 2006; Skilling, 2006), such as the difference in accumulated evidence between successive iterations, difference in the likelihood value between discarded samples, or the amount of remaining live evidence. Following the termination, the $K$ stored samples are used to estimate the evidence via:

$$\mathcal{Z} = \sum_{k=1}^{K} \mathcal{L}_k\, \Delta\varepsilon_k, \tag{31}$$

with

$$\Delta\varepsilon_k = \varepsilon_{k-1} - \varepsilon_k. \tag{32}$$

Additionally, the sequence of discarded samples may be considered as a Monte Carlo sequence from the posterior. By weighting each sample according to its area of contribution to $\mathcal{Z}$ with weight:

$$w_k = \frac{\mathcal{L}_k \, \Delta\varepsilon_k}{\mathcal{Z}}, \tag{33}$$

Monte Carlo estimates of posterior properties can be readily obtained. For instance, the parameter mean values may be calculated as

$$\mu(\boldsymbol{\theta}) = \sum_{k=1}^{K} w_k \, \boldsymbol{\theta}_k \tag{34}$$

and the parameter standard deviations as

$$\sigma(\boldsymbol{\theta}) = \left[ \sum_{k=1}^{K} w_k \left( \boldsymbol{\theta}_k - \mu(\boldsymbol{\theta}) \right)^2 \right]^{1/2}. \tag{35}$$

## IV. BAYESIAN ANALYSIS RESULTS

To ensure accurate and efficient computation, the nested sampling procedure must be tuned to the specific needs of each application. More specifically to this work, the multi-layer porous material inversion task involves a moderately-high dimensional parameter space (four parameters per layer with the generalized Miki (1990) model) over a broad range of parameter values. Additionally, as will be demonstrated in the remainder of this section, the parameter space may be multimodal, particularly for material layers beyond the surface layer. To ensure an adequate coverage of the parameter space and to reduce the potential for fluctuations in the evidence and posterior estimates due to the multimodality, a population of $Q = 500$ live samples is used in the results reported here.

At each iteration of the nested sampling implementation, replacement samples are generated by evolving a random survivor sample via a random walk Metropolis-Hastings procedure (Skilling, 2006). Steps are accepted if they result in a likelihood value greater than the constraint and rejected otherwise. For each replacement sample, 25 accepted steps are required, with the step size adjusted as in Skilling (2006).

Since likelihood function and evidence values can become quite large, the nested sampling procedure is implemented on a logarithmic scale to avoid the potential for numerical overflow errors. Sampling iterations are terminated when the current iteration's live evidence (Keeton, 2011) can contribute no more than 0.05 to the currently accumulated evidence and when the maximum difference in log likelihood between any two live population samples is less than 0.5.

### A. Measured surface impedance

For the results reported in the remainder of this paper, the material under test consists of single-layer and two-layer combinations of melamine foam and Armafoam Sound (AFS) 240 foam. The data $\boldsymbol{\mathcal{D}}$ used for studying the porous materials consisted of normal-incidence complex acoustic surface impedance, measured in a 29 mm diameter impedance tube using the transfer-function method (Chung and Blaser, 1980; International Standards Organization, 1998).

To study the applicability of the method under varying material compositions, the two-layer sample was measured in two orientations, with both the melamine foam and the AFS

foam forming the top layer in turn. Figure 1 illustrates the measured surface impedance for both orientations.

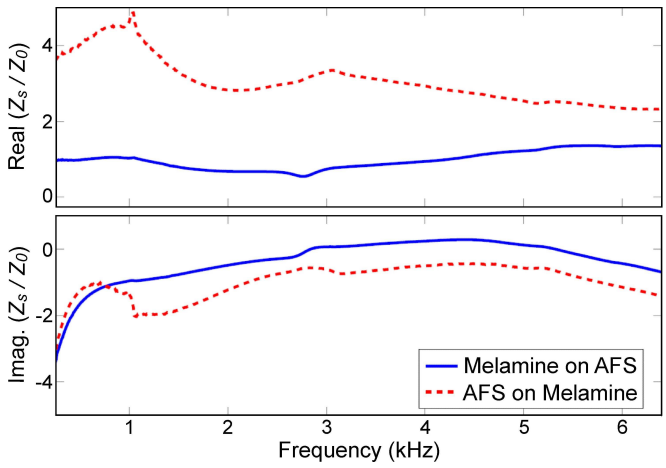


FIG. 1. (Color online) Experimentally measured, specific normal incident surface impedance of two layers of porous materials as function of frequency. Solid-line: Armafoam sound 204 foam behind Melamine foam with the later being exposed to the incident sound. Dotted-line: Melamine foam behind Armafoam sound 204 foam with the later being exposed to the incident sound.

### B. Determination of layers present

Bayes factors were employed to determine the number of layers present in the porous sample under test. In the present work, a simpler model (one with fewer porous layers) is always preferred if it yields a positive Bayes factor (higher evidence value) when compared to a more complex model. Additionally, if the Bayes factor comparing two models is less than 20 dBans, the simpler model is preferred.

Given the measured surface impedance data for the orientation with the melamine foam layer on top and considering the layer thickness as a free parameter, the Bayesian evidence

TABLE I. Evidence values and Bayes factors for combinations of melamine foam and AFS foam varying the number of layers present in a multilayer formulation. Evidence values $\mathcal{Z}_i$ for the model with $i$ layers presented logarithmically, as the mean ± standard deviation from four nested sampling runs. Bayes factors $\mathcal{K}_{i,i-1}$ comparing the model with $i$ layers to that with $i-1$ layers calculated from the mean log evidence and presented to the nearest decibans.

| # Layers (Melamine on AFS) | Log Evidence ± deviations (dBans) | $\mathcal{K}_{i,i-1}$ (dBans) |
|---|---|---|
| 1 | -2902.8 ± 1.3 | – |
| 2 | 2137.2 ± 13.0 | 5040 |
| 3 | 2152.8 ± 26.5 | 16 |
| 4 | 2106.8 ± 23.5 | -46 |
| **# Layers (AFS on Melamine)** | **Log Evidence ± deviations (dBans)** | **$\mathcal{K}_{i,i-1}$ (dBans)** |
| 1 | -2491.1 ± 0.9 | – |
| 2 | -1237.7 ± 2.6 | 1253 |
| 3 | -1191.7 ± 45.2 | 46 |
| 4 | -1193.9 ± 43.0 | -2 |

is computed for models considering various numbers of layers (1-4), including two different layer orientations. In addition to the models of 1- and 2-layers, overparameterized models, namely 3- and 4-layers are intentionally tested to evaluate how the Bayesian evidence behaves for these models.

Table I lists these evidence values given by Equation (31) estimated using the nested sampling. With increasing number of layers, from 2-layers no significant increase of the logarithmic evidence can be observed. These lead to the selection of a two-layer model, consistent with what is physically expected, knowing a two-layer sample provided the measured data. Since fixing the thickness of the individual layers led to non-realistic thicknesses of the overall material sample for any combination other than the two layers actually present, a two-layer model is used and the evidence are not tabulated for the fixed-thickness case.

In the case when the AFS 240 foam layer is on the top of melamine foam, the effect of the first layer becomes dominant. The evidence values listed in Table I indicates that any of these (4) models with the intended orientation does not physically agree with the measured two-layer material setting. For this reason, no further results are reported for this particular case. Moreover, considering the parameter value reported in Table II, the AFS 240 foam layer has a flow resistivity greater than 10 times of that for the melamine foam. It indicates that the porous material layer with significantly higher flow resistivity as the surface layer seems to overshadow the layers of lower flow resistivity behind it. A potential for future work would be to study this situation in further detail, in an attempt to discern the limitations of the diverse porous parameters for those multilayer materials in which the pore stratification is particularly pronounced.

### C. Parameter estimation for two-layer material

In addition to the evidence used to determine the number of material layers present in the sample, the nested sampling procedure implemented according to Section III E pro-

duces samples from the posterior probability distribution. This distribution quantifies the knowledge gained about the parameters describing the macroscopic pore structure.

Focusing on the two-layer model (as selected by the evidence described in Section IV B), the posterior distribution has eight dimensions: for each of the two layers, three dimensions correspond to the physical parameters of the Miki generalized model, with an additional dimension for the layer thickness. For the sake of visualization in this paper, the posterior distribution samples are plotted as marginalized views along each possible combination of two dimensions.

Figures 2 plots the posterior distribution samples while focusing on the dimensions relevant for the melamine foam and AFS foam layers, respectively. Figure 3 shows the dimensions of the posterior distribution describing both layers simultaneously. In each of these figures, the samples output from the nested sampling process are plotted with color indicating the logarithmic posterior probability density. Regions of highest posterior probability indicate the most likely parameter values, in light of the experimentally-measured surface impedance data.

Each subplot within the figures concentrates on the relationship between two parameters. For example, Figure 2 (a) shows the posterior dimensions of flow resistivity (abscissa) and thickness (ordinate) of the melamine foam layer. The top-right subplot of Figure 3 shows the covariance between the tortuosity of the AFS foam layer (abscissa) and the thickness of the melamine foam layer (ordinate).

The posterior distribution samples are also used to estimate the mean value and standard deviation of each parameter, via Equations (34) and (35). Table II lists these estimates, as

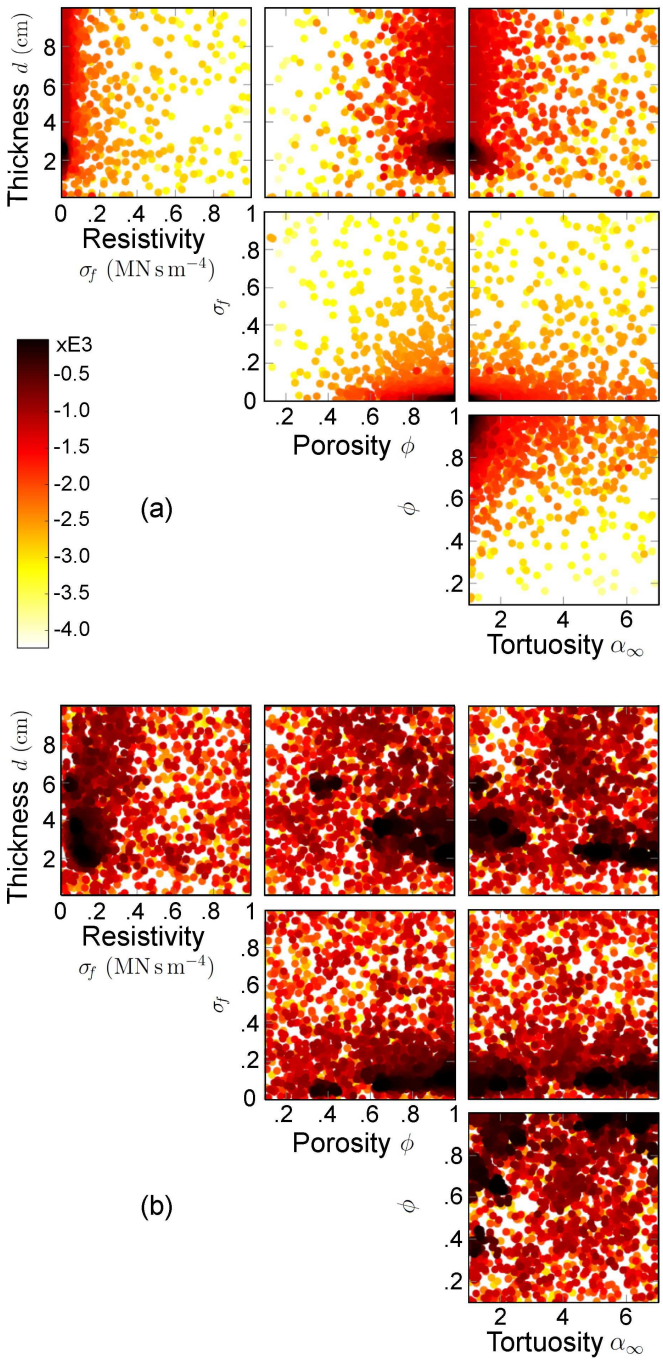


FIG. 2. (Color online) Marginal logarithmic posterior samples for melamine foam layer (a) and AFS foam layer (b). Every fifth sample from the nested sampling procedure is plotted with color proportional to logarithmic posterior probability density. Parameters shown include layer thickness $d$, flow resistivity $\sigma_f$, porosity $\phi$, and tortuosity $\alpha_\infty$. (a) Layer 1 (melamine foam). (b) Layer 2 (AFS 240 foam).

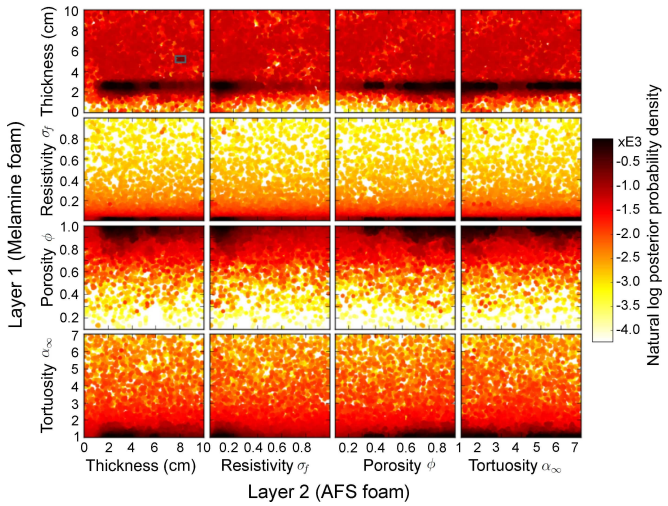


FIG. 3. (Color online) Marginal logarithmic posterior samples, showing the interaction between the melamine and AFS foam layers. As in Figure 2, each sample from the nested sampling procedure is plotted with color proportional to logarithmic posterior probability density. The parameters shown include layer thickness $d$, flow resistivity $\sigma_f$, porosity $\phi$, and tortuosity $\alpha_\infty$.

estimated from the posterior samples plotted in Figures 2 (a), 2 (b) through Figure 3 for the two-layer case of melamine foam on AFS foam.

To study the ability of the Bayesian analysis to determine the thickness of the constituent layers, two posterior distributions are determined. In the first, the layer thickness is considered as an unknown free parameter and estimated from the data along with the other physical parameters. In the second case, only the Miki model parameters are estimated from the data, while the layer thickness is measured physically and fixed at its known value. While only the posterior distribution with layer thickness as a free parameter is plotted, Table II also includes the posterior parameter estimates from the case where the layer thickness is fixed at its actual value.

TABLE II. Estimated parameter values (mean ± standard deviation) based on measured data for the acoustic surface impedance for the combination of melamine foam on AFS 240 foam. Two-layer fit is obtained using the 3-parameter Miki generalized model. The layer thickness is estimated from measured acoustic data (top) and fixed at the known value (bottom). Directly measured flow resistivity, $\sigma_f$, and porosity, $\phi$, from a Round Robin Test (Horoshenkov *et al.*, 2007) are also listed for ease of comparison.

| Layer (Sampled Thickness) | Melamine | AFS 240 |
|---|---|---|
| Layer Thickness, $d$ (cm) | 2.60 ± 0.01 | 2.39 ± 0.26 |
| Flow Resistivity, $\sigma_f$ (Ns/m$^4$) | 7,360 ± 140 | 108,200 ± 8,380 |
| (Directly measured), $\sigma_f$ (Ns/m$^4$) | 9,900 ± 800 | 141,400 ± 44,000 |
| Porosity, $\phi$ | 1.00 ± 0.00 | 0.96 ± 0.07 |
| (Directly measured), $\phi$ | 0.98 ± 0.01 | 0.80 ± 0.02 |
| Tortuosity, $\alpha_\infty$ | 1.00 ± 0.00 | 5.07 ± 0.62 |
| **Layer (Fixed Thickness)** | **Melamine** | **AFS 240** |
| Layer Thickness (cm) | 2.50 | 2.50 |
| Flow Resistivity, $\sigma_f$ (Ns/m$^4$) | 8,050 ± 160 | 108,260 ± 2,420 |
| (Directly measured), $\sigma_f$ (Ns/m$^4$) | 9,900 ± 800 | 141,400 ± 44,000 |
| Porosity, $\phi$ | 1.00 ± 0.00 | 0.93 ± 0.01 |
| (Directly measured), $\phi$ | 0.98 ± 0.01 | 0.80 ± 0.02 |
| Tortuosity, $\alpha_\infty$ | 1.01 ± 0.01 | 4.16 ± 0.10 |

457 Table II indicates, the parameter standard deviations for layer 2 are larger than those for
458 layer 1. This agrees with what might be physically expected, since the acoustic waves used
459 to measure the material's surface impedance must propagate through the first layer before
460 encountering the second layer. In addition to the larger standard deviation estimates, the
461 larger uncertainty in the layer 2 parameter values is seen in the plotted posterior distribution.
462 The effect is particularly evident in Figure 3, where the distribution is much broader along
463 the dimensions corresponding to the second layer than along the dimensions for the first
464 layer.

465 Note that the material samples used in this work are the same as those tested in the Round
466 Robin experiments (Horoshenkov *et al.*, 2007; Pompoli *et al.*, 2017). The non-acoustically
467 measured values of the porosity and flow resistivity (Horoshenkov *et al.*, 2007) for melamine
468 foam are $9.9 \pm 0.8$ kPa s m$^{-2}$ and $0.98 \pm 0.01$, respectively. For AFS 240 foam, these values
469 are $141.4 \pm 44.0$ kPa s m$^{-2}$ and $0.80 \pm 0.02$, respectively. Table II also lists these values
470 for ease of comparison. In Table II, the porosity being close to 1.0 actually indicates a high
471 enough value, as high as 0.98. It is straightforward to demonstrate that for a material such
472 as melamine foam the porosity is high enough and it does not control the measured acoustic
473 behavior. This may be the reason why models such as the Delany and Bazley (1970) and
474 the original model by Miki (1990) neglect the porosity and tortuosity.

475 To validate the physical parameter values obtained from the Bayesian inversion procedure,
476 these estimated parameter values are used to model the surface impedance of the two-layer
477 material. This model is then compared to the experimentally-measured surface impedance
478 data. Figure 4 shows the measured complex surface impedance data and two-layer Miki

(1990) generalized model fit obtained with the estimated parameter values. The agreement between the measured and modeled results becomes evident. These are achieved using the estimated parameter values.

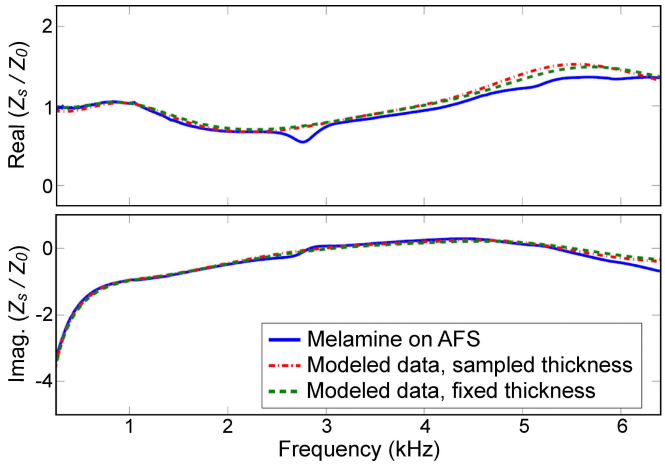


FIG. 4. (Color online) Measured and modeled surface impedances of two layered porous forms with Melamine on on top of AFS 204 foam. In the Bayesian model-based estimation, the layer thickness is kept either as a fixed known value (2.5 cm), or as an unknown parameter.

## V. CONCLUSIONS

A Bayesian model-based acoustic method for inversely determining the pore microstructure of multilayer porous media from the acoustic impedance data has been presented. This work shows that the method simultaneously determines the number of layers present in a two-layer sample, as well as the physical properties of each constituent layer. The nested sampling algorithm is used to perform the numerical calculations and to provide estimates of the Bayesian evidence and samples from the posterior distribution. The obtained evidence

provides a quantitative method of model selection for determining the number of layers in a material under test, while the posterior distribution quantifies the knowledge gained about the layers' physical properties. The method is demonstrated with the analysis of a two-layer combination of melamine foam and Armafoam Sound 240 foam. The method requires further development to extend it to those materials which consist of porous layer with strong functional gradient. Specifically, it is impossible to determine accurately the layer composition of the sample which consisted of the low permeability AFS 240 foam layer installed on the specimen's top.

## VI. ACKNOWLEDGMENT

The authors are grateful to Dr. Amir Khan (University of Bradford, UK) for taking impedance measurements on the materials investigated.

Allard, J. F. and Atalla, N. (**2009**). *Propagation of Sound in Porous Media: Modelling Sound Absorbing Materials*, second edition (John Wiley & Sons, Ltd, West Sussex, UK), pp. 15–27, 45–109, 243–281.

Allard, J. F., Castagnede, B., Henry, M., and Lauriks, W. (**1994**). "Evaluation of tortuosity in acoustic porous materials saturated by air," Rev. Sci. Instrum. **65**, 754–755.

Atalla, Y. and Panneton, R. (**2005**). "Inverse acoustical characterization of open cell porous media using impedance tube measurements," Can. Acoust. **33**, 11–24.

508 Attenborough, K. (**1985**). "Acoustical impedance models for outdoor ground surfaces," J.
509 Sound Vib. **99**, 521 – 544.

510 Battle, D. J., Gerstoft, P., Hodgkiss, W. S., Kuperman, W. A., and Nielsen, P. L. (**2004**).
511 "Bayesian model selection applied to self-noise geoacoustic inversion," J. Acoust. Soc. Am.
512 **116**, 2043–2056.

513 Beaton, D. and Xiang, N. (**2017**). "Room acoustic modal analysis using Bayesian inference,"
514 J. Acoust. Soc. Am. **141**, 4480–4493.

515 Beranek, L. L. (**2004**). *Concert Halls and Opera Houses: Music, Acoustics and Architecture*
516 *(Chapter 4)*, second edition (Springer, New York).

517 Betancourt, M. (**2011**). "Nested sampling with constrained Hamiltonian Monte Carlo," in
518 *Bayesian Inference and Maximum Entropy Methods in Science and Engineering*, edited by
519 A. Mohammad-Djafari, J.-F. Bercher, and P. Bessiere, volume 165, 165–172.

520 Botts, J. M., Escolano, J., and Xiang, N. (**2013**). "Design of IIR filters with Bayesian model
521 selection and parameter estimation," IEEE Trans. Audio, Speech, Language Process. **21**,
522 669–674.

523 Buckingham, M. J. (**2000**). "Wave propagation, stress relaxation, and grain-to-grain shear-
524 ing in saturated, unconsolidated marine sediments," J. Acoust. Soc. Am. **108**, 2796–2815.

525 Bush, D. and Xiang, N. (**2018**). "A model-based bayesian framework for sound source
526 enumeration and direction of arrival estimation using a coprime microphone array," J.
527 Acoust. Soc. Am. **143**, 3934–3945.

528 Chan, C.-Y. and Goggans, P. (**2012**). "Using Bayesian inference for the design of FIR filters
529 with signed power-of-two coefficients," Signal Process. **92**, 2866–2873.

Chazot, J.-D., Zhang, E., and Antoni, J. (**2012**). "Acoustical and mechanical characterization of poroelastic materials using a Bayesian approach," J. Acoust. Soc. Am. **131**, 4584–4595.

Chevillotte, F., Jaouen, L., and Becot, F.-X. (**2015**). "On the modeling of visco-thermal dissipations in heterogeneous porous media," J. Acoust. Soc. Am. **138**, 3922–3929.

Chung, J. Y. and Blaser, D. A. (**1980**). "Transfer function method of measuring in-duct acoustic properties. I. Theory," J. Acoust. Soc. Am. **68**, 907–913.

Delany, M. E. and Bazley, E. N. (**1970**). "Acoustical properties of fibrous absorbent materials," Appl. Acoust. **3**, 105–116.

Dettmer, J., Dosso, S. E., and Holland, C. W. (**2009**). "Model selection and Bayesian inference for high-resolution seabed reflection inversion," J. Acoust. Soc. Am. **125**, 706–716.

Dettmer, J., Dosso, S. E., and Holland, C. W. (**2010**). "Trans-dimensional geoacoustic inversion," J. Acoust. Soc. Am. **128**, 3393–3405.

Escolano, J., Perez-Lorenzo, J. M., Xiang, N., Cobos, M., and López, J. J. (**2012**). "A Bayesian inference model for speech localization (L)," J. Acoust. Soc. Am. **132**, 1257–1260.

Escolano, J., Xiang, N., Perez-Lorenzo, J. M., Cobos, M., and Lopez, J. J. (**2014**). "A Bayesian direction-of-arrival model for an undetermined number of sources using a two-microphone array," J. Acoust. Soc. Am. **135**, 742–753.

Horoshenkov, K. V., Khan, A., Bécot, F.-X., Jaouen, L., Sgard, F., Renault, A., and Amirouche, N. (**2007**). "Reproducibility experiments on measuring acoustical properties

552 of rigid-frame porous media (round-robin tests)," J. Acoust. Soc. Am. **122**, 345–353.

553 Horoshenkov, K. V., Khan, A., and Benkreira, H. (**2013**). "Acoustic properties of low grow-
554 ing plants," J. Acoust. Soc. Am. **133**, 2554–2565.

555 International Standards Organization (**1998**). *ISO 10534-2 Acoustics – Determination of*
556 *sound absorption coefficient and impedance in impedance tubes – Part 2: Transfer-function*
557 *method* (International Standards Organization, Geneva).

558 Jasa, T. and Xiang, N. (**2009**). "Efficient estimation of decay parameters in acoustically
559 coupled spaces using slice sampling," J. Acoust. Soc. Am. **126**, 1269–1279.

560 Jaynes, E. (**1968**). "Prior probabilities," IEEE Trans. Syst. Sci. Cybern. **4**, 227–241.

561 Jefferys, W. H. and Berger, J. O. (**1992**). "Ockham's razor and Bayesian analysis," Am.
562 Sci. **80**, 64–72.

563 Jeong, C.-H., Choi, S.-H., and Lee, I. (**2017**). "Bayesian inference of the flow resistivity of
564 a sound absorber and the rooms influence on the sabine absorption coefficients (L)," J.
565 Acoust. Soc. Am. **141**, 1711–1714.

566 Kass, R. E. and Raftery, A. E. (**1995**). "Bayes factors," J. Am. Stat. Assoc. **90**, 773–795.

567 Keeton, C. R. (**2011**). "On statistical uncertainty in nested sampling," Mon. Not. R. Astron.
568 Soc. **414**, 1418–1426.

569 Leurer, K. C. and Brown, C. (**2008**). "Simplified porosity measurements," J. Acoust. Soc.
570 Am. **123**, 1941–1951.

571 Long, M. (**2014**). *Architectural Acoustics*, second edition (Elsevier, Oxford, UK).

572 MacKay, D. J. C. (**2003**). *Information Theory, Inference, and Learning Algorithms* (Cam-
573 bridge University Press, Cambridge, UK), pp. 343–355.

574 Mahasaranon, S., Horoshenkov, K. V., Khan, A., and Benkreira, H. (**2012**). "The effect
575 of continuous pore stratification on the acoustic absorption in open cell foams," J. Appl.
576 Phys. **111**, 084901.
577 Miki, Y. (**1990**). "Acoustical properties of porous materials—Generalizations of empirical
578 models," J. Acoust. Soc. Jpn. **11**, 25–28.
579 Niskanen, M., Groby, J.-P., Duclos, A., Dazel, O., Roux, J. C. L., Poulain, N., Huttunen,
580 T., and Lhivaara, T. (**2017**). "Deterministic and statistical characterization of rigid frame
581 porous materials from impedance tube measurements," J. Acoust. Soc. Am. **142**, 2047–
582 2418.
583 Ogam, E., Depollier, C., and Fellah, Z. E. A. (**2010**). "The direct and inverse problems of
584 an air-saturated porous cylinder submitted to acoustic radiation," Rev. Sci. Instrum. **81**,
585 094902–1–094902–9.
586 Pompoli, F., Bonfiglio, P., Horoshenkov, K. V., Khan, A., Jaouen, L., Becot, F.-X., Sgard,
587 F., Asdrubali, F., D'Alessandro, F., Huebelt, J., Atalla, N., Amedin, C. K., Lauriks, W.,
588 and Boeckx, L. (**2017**). "How reproducible is the acoustical characterization of porous
589 media?," J. Acoust. Soc. Am. **141**, 945–955.
590 Sabatier, J. M., Bass, H. E., and Bolen, L. N. (**1986**). "The interaction of airborne sound
591 with the porous ground: The theoretical formulation," J. Acoust. Soc. Am. **79**, 1345–1352.
592 Sabatier, J. M. and Xiang, N. (**2001**). "An investigation of acoustic-to-seismic coupling to
593 detect buried antitank landmines," IEEE Trans. Geosci. Remote Sens. **39**, 1146–1154.
594 Sivia, D. S. and Skilling, J. (**2006**). *Data analysis: A Bayesian tutorial*, second edition
595 (Oxford University Press, Oxford, UK), pp. 103–126, 181–208.

Skilling, J. (**2004**). "Nested sampling," in *Bayesian Inference and Maximum Entropy Methods in Science and Engineering*, volume 735 of *AIP Conference Proceedings*, Garching, Germany, 25–30 July 2004, pp. 395–405.

Skilling, J. (**2006**). "Nested sampling for general Bayesian computation," Bayesian Anal. **1**, 833–859.

Xiang, N. (**2015**). "Advanced room-acoustics decay analysis," in *Acoustics, Information, and Communication: Memorial Volume in Honor of Manfred R. Schroeder*, edited by N. Xiang and G. M. Sessler (Springer, Cham, Switzerland), Chap. 3, pp. 33–56.

Xiang, N. and Fackler, C. (**2015**). "Objective Bayesian analysis in acoustics," Acoust. Today **11**, 54–61.

Xiang, N. and Goggans, P. M. (**2003**). "Evaluation of decay times in coupled spaces: Bayesian decay model selection," J. Acoust. Soc. Am. **113**, 2685–2697.

.

609 ## Caption

610 Figure 1. (Color online) Experimentally measured, specific normal incident surface impedance
611 of two layers of porous materials as function of frequency. Solid-line: Armafoam sound 204
612 foam behind Melamine foam with the later being exposed to the incident sound. Dotted-
613 line: Melamine foam behind Armafoam sound 204 foam with the later being exposed to the
614 incident sound.

615 Figure 2. (Color online) Marginal logarithmic posterior samples for melamine foam layer
616 in (a) and AFS foam layer in (b). Every fifth sample from the nested sampling procedure
617 is plotted with color proportional to logarithmic posterior probability density. Parameters
618 shown include layer thickness $d$, flow resistivity $\sigma_f$, porosity $\phi$, and tortuosity $\alpha_\infty$. (a) Layer
619 1 (melamine foam). (b) Layer 2 (AFS 240 foam).

620 Figure 3. (Color online) Marginal logarithmic posterior samples, showing the interaction
621 between the melamine and AFS foam layers.

622 Figure 4. (Color online) Measured and modeled surface impedances of two layered porous
623 forms with Melamine on on top of AFS 204 foam. In the Bayesian model-based estima-
624 tion, the layer thickness is kept either as a fixed known value (2.5 cm), or as an unknown
625 parameter.

TABLE I. Evidence values and Bayes factors for combinations of melamine foam and AFS foam varying the number of layers present in a multilayer formulation. Evidence values $\mathcal{Z}_i$ for the model with $i$ layers presented logarithmically, as the mean $\pm$ standard deviation from four nested sampling runs. Bayes factors $\mathcal{K}_{i,i-1}$ comparing the model with $i$ layers to that with $i-1$ layers calculated from the mean log evidence and presented to the nearest decibans.

TABLE II. Estimated parameter values (mean $\pm$ standard deviation) based on measured data for the acoustic surface impedance for the combination of melamine foam on AFS 240 foam. Two-layer fit is obtained using the 3-parameter Miki generalized model. The layer thickness is estimated from measured acoustic data (top) and fixed at the known value (bottom). Directly measured flow resistivity, $\sigma_f$, and porosity, $\phi$, from a Round Robin Test (Horoshenkov *et al.*, 2007) are also listed for ease of comparison.